To Sink, Swim, Twin, or Nucleate: A critical appraisal of crystal aggregation processes

Penny E. Wieser[1*], Zoja Vukmanovic[1], Rüdiger Kilian[2], Emilie Ringe[1,3], Marian B. Holness[1], John Maclennan[1], Marie Edmonds[1]

[1] Department of Earth Sciences, University of Cambridge, UK.

[2] Institute for Geosciences and Geography, University Halle, Germany

[3]Department of Materials Science and Metallurgy, University of Cambridge, UK.

* Corresponding author: pew26@cam.ac.uk

ABSTRACT

Crystal aggregates in igneous rocks have been variously ascribed to growth processes (e.g., twinning, heterogeneous nucleation, epitaxial growth, dendritic growth), or dynamical processes (e.g., synneusis, accumulation during settling). We tested these hypotheses by quantifying the relative orientation of adjacent crystals using Electron Backscatter Diffraction. Both olivine aggregates from Kīlauea Volcano (Hawai'i, USA) and chromite aggregates from the Bushveld Complex (South Africa) show diverse attachment geometries inconsistent with growth processes. Near-random attachments in chromite aggregates are consistent with accumulation by settling of individual crystals. Attachment geometries and prominent geochemical differences across grain boundaries in olivine aggregates are indicative of synneusis.

INTRODUCTION

Despite the abundance of crystal aggregates in a diverse range of igneous rocks, no consensus has been reached on their origin (Day and Taylor, 2007; Jerram et al., 2003; Schwindinger and Anderson, 1989). As early as 1921, Vogt suggested that crystal aggregates form by synneusis, the "swimming together" and attachment of previously isolated crystals in a fluid medium. More recently, aggregates have been attributed to growth twinning (Welsch et al., 2013), the nucleation and growth of a daughter crystal via epitaxial growth/heterogeneous nucleation (Dowty, 1980a; Hammer et al., 2010; Kirkpatrick, 1977; Špillar and Dolejš, 2015), or the textural maturation of dendrites (Welsch et al., 2013; 2014). Previous attempts at distinguishing these hypotheses have utilized optical observations of chemical zoning (Dowty, 1980a), assessments of crystallographic orientation using a universal stage (Ross, 1957), and observations of 3D aggregate morphology (Schwindinger and Anderson, 1989; Welsch et al., 2013). In this study, we quantied changes in crystallographic orientation across grain boundaries using Electron Backscatter Diffraction maps (EBSD; e.g., Prior et al., 1999). This allows direct comparison between observed

aggregate geometries and those predicted by each hypothesis, even in optically isotropic or chemically homogeneous minerals. To demonstrate the versatility of this method, we investigate olivine aggregates from rapidly quenched scoria from several eruptions at Kīlauea Volcano, Hawai'i, USA A.D. ca. 1700, ca. 1920, and 1969–1975; see DR1 in the GSA Data Repository1 41 ; Fig. 1) and chromite crystals from the UG2 chromitite layer of the Bushveld Complex, South Africa (Fig. 2).

Unravelling the magmatic processes responsible for aggregation has important implications. At Kīlauea, olivine constitutes the principal record of pre-eruptive processes in primitive lavas. Understanding the formation and evolution of chromitite layers such as the Bushveld UG2 is crucial to advance our understanding of how platinum group elements are concentrated into economically viable ore deposits (Naldrett, 2013). The timing and mechanism of aggregate formation also influences crystal re-distribution and accumulation in layered intrusions (Campbell, 1978; Holness et al., 2017a), and the interpretation of quantitative textural measurements such as crystal size distributions (CSDs), which frequently record kinked CSDs, and an over-abundance of larger crystal sizes in volcanic rocks (Marsh, 1998).

METHODS & RESULTS

EBSD maps were made for 93 Kīlauean aggregates (Fig. 1) and a thin section of the UG2 layer of the Bushveld Complex containing ~3500 chromite grains (Fig. 2). The crystallographic relationships between touching grains in aggregates were quantified in terms of their misorientation. This describes the coordinate transform from one crystal orientation to that across the grain boundary, displayed as an axis-angle pair (Fig. 3a). Misorientations were calculated using MTEX V5.0.4 (Bachmann et al., 2010), an open-source toolbox for MATLAB. Electron microprobe transects across olivine aggregates were obtained using a Cameca SX100 electron probe microanalyzer (EPMA; see DR1).

Olivine aggregates, consisting of 2-17 individual crystals (Fig. 1), showed misorientation axes strongly clustered about <100> (Fig. 3b), and broad peaks in misorientation angles at <5˚, ~40˚ and ~80˚ (Fig. 3c). EPMA transects across attached olivine crystals reveal flat compositional profiles in the cores of crystals, with sharp gradients across grain boundaries (Fig. 1e; sections X-X', Z-Z'). The distribution of chromite misorientation angles was very close to the theoretical random distribution (Fig. 4c), with the only prominent peak at 60˚. Chromite misorientation axes exhibited weak clustering about <111> and <011> (Fig. 4a). Removal of the {111} twins responsible for the 60˚ peak results in a nearly uniform distribution of misorientation axes and angles (Fig. 4b-c).

PHYSICAL AGGREGATION OF CRYSTALS

Hydrodynamic processes within magmatic systems can drive the aggregation of preformed crystals (McIntire et al., 2019). One such process is synneusis (Vogt, 1921; Vance, 1969). While the driving forces associated with interfacial energy minimisation during synneusis are too localized to drive crystals together (Dowty, 1980a), crystals may be aligned while suspended in convecting magma (Holness et al., 2017b), or during settling (Schwindinger, 1999; Schwindinger and Anderson, 1989), resulting in their attachment in specific orientations. Once sufficiently close, reductions in interfacial energy associated with particular crystallographic orientations can drive small readjustments in aggregate geometry (Dowty, 1980a), before further crystal growth cements the crystals together.

To assess the synneusis hypothesis in Kilauean olivine aggregates, the faces of attachment between adjacent crystals were assessed by superimposing 3D olivine shapes onto EBSD maps using the crystalShape MTEX class (Enderlein, 1997; https://mtex-toolbox.github.io/files/doc/crystalShape_index.html; Fig. 1c), and these were compared to the predicted hydrodynamical alignments during settling. Oblate olivines align their axis of symmetry vertically during settling, while prolate olivines align their axis of symmetry horizontally (Leal, 1980). This creates mostly {010} attachments in oblate olivines, and {110} attachments in prolate olivines, with occasional {021} attachments in both cases (Schwindinger and Anderson, 1989). We anticipate that similar alignments would also occur during convection.

The {110}-{110} attachments were the most commonly observed geometry in Kīlauean aggregates (Fig. 1c), followed by {010}-{010} or parallel {021}-{021} attachments (difficult to distinguish in 2D). Crystals which are perfectly attached along parallel {110}-{110}, {010}-{010} and {021}-{021} faces would have identical orientations, while perfect attachments along {021}-{010} and perpendicular {021}-{021} faces would generate misorientations about <100> of 40.4˚ and 80.9 ˚ respectively. The presence of broad misorientation angle peaks centred about these angles is strong evidence for synneusis (Fig. 3c). Unlike crystal growth processes, which favour specific crystallographic relationships, attachment by synneusis can easily generate misalignments from these ideal attachment geometries, through the mechanical hindrance to re-orientation driven by the reduction of interfacial energies (Nespolo and Ferraris, 2004; Vance, 1969), or near-random attachment under conditions of high supersaturation (Schwindinger and Anderson, 1989). Imperfect attachment by synneusis also accounts for the presence of discontinuous melt films between adjacent

olivine crystals (Fig. 1a-b). If formed during growth, such films would impose high energy penalties.

Finally, EPMA transects support the hypothesis that the olivine aggregates formed by synneusis (Fig. 1e). While synneusis can bring together crystals with different core compositions that formed in disparate environments (Schwindinger and Anderson, 1989), aggregates produced by twinning or dendritic growth share a common history, so the cores of attached crystals should have identical chemistry (Philpotts et al., 1998). The sharp gradients in forsterite contents (which dissipate rapidly by diffusion) suggest that the aggregation event occurred shortly before eruption. Crystal aggregation may occur following a disturbance to the magmatic system triggering their eruption, or during transport of the magma to the eruption site.

Evaluating the role of physical aggregation in the formation of chromite aggregates is complicated because attachment along the only crystal face, {111}, produces misorientation axes indistinguishable from primary twinning (60˚ rotation about <111>; Deer, 1966). However, this geometric relationship is relatively uncommon, and the removal of misorientations corresponding to the chromite twin law (and effects induced by crystal symmetry) produces a near-uniform misorientation axis distribution, and an angle distribution resembling the theoretical random distribution (Fig. 4b-c). This implies that chromite grains are randomly aggregated by a mechanism which is not selective to crystallographic orientation; this is inconsistent with the attachment of {111} faces by synneusis, or various growth processes. We suggest that the randomly-oriented touching frameworks of chromite grains formed during the settling of individual grains through the overlying magma column to the top of the cumulate pile (Jackson, 1961). This hypothesis is consistent with microstructures in the cumulates overlying UG2, in which individual chromite grains apparently rest on underlying pyroxene primocrysts (Fig. 2c).

CRYSTAL GROWTH PROCESSES

Crystal aggregates attached along specific planes have also been attributed to primary twinning (Welsch et al., 2013). However, neighbouring chromite grains displaying twin relations are relatively rare (<10% of neighbouring grains, based on deviations from ideal twin laws; Brandon, 1966; DR1). Similarly, <7% of neighbouring olivines are related by the three olivine twin laws (twinning on {011}, {012} and {031}, corresponding to misorientations

about <100> of 60.7˚, 32.6˚ and 59.3˚ respectively; Azevedo and Nespolo, 2016; Dodd and Calef, 1971). Thus, twinning is not the dominant cause of grain aggregation in our samples.

Dowty (1980a) suggested that the textural and chemical characteristics of crystal aggregates could result from epitaxial growth or heterogeneous nucleation. These processes, driven by the reduction of the activation barrier to nucleation by the presence of an existing crystalline substrate in the melt (Lofgren, 1983; Mithen and Sear, 2014), are well-documented in multiphase aggregates (Hammer et al., 2010; Kirkpatrick, 1977). However, in monomineralic aggregates, nucleation and growth of a daughter crystal are associated with energy penalties. The increased surface area per unit volume (and increased interfacial energy) caused by the growth of a daughter crystal was assessed by comparing an individual crystal of a given volume with an aggregate with the same total volume composed of two identical crystals (volumes and areas calculated in SHAPE7.4; Dowty, 1980b; DR1). As chromite crystals express only {111} faces, the increase in interfacial energy for aggregates compared to individual crystals (11%) is independent of the interfacial energy of the {111} face. For olivine, theoretical surface energies for the 6 different olivine faces in a vacuum at 0 K (Bruno et al., 2014) were used. Regardless of the attachment face, the growth of a daughter crystal in olivine is accompanied by significant energy penalties (13-24%; see DR1).

Energy penalties for heterogenous nucleation are even greater. While epitaxial growth describes the nucleation of crystals in a specific crystallographic orientation with respect to the host crystal (identical or twin orientations in single phase aggregates; Mithen and Sear, 2014), heterogeneous nucleation has no such orientation constraints. The large lattice mismatches, and associated energy penalties, generated by heterogeneous nucleation may drive the detachment of a poorly-orientated unit, followed by reattachment in a more favourable orientation (Buerger, 1945). In certain cases, it may even be more energetically favourable for the components of the misaligned daughter crystal to remain in the liquid state (Brugger and Hammer, 2015).

The larger energy penalties for heterogeneous nucleation than epitaxial growth, alongside lower nucleation rates for mismatching parent and daughter lattices (Turnbull and Vonnegut, 1952), means that heterogeneous nucleation should occur less frequently than epitaxy in monomineralic aggregates. Olivine and chromite aggregates show little evidence for epitaxy; twin relationships are rare (Fig. 3-4), and no crystals with uniform orientations show external

morphologies indicative of aggregation. Given the limited evidence for epitaxial growth, it is improbable that the energetically unfavourable process of heterogeneous nucleation was the dominant cause of grain aggregation in this study.

Welsch et al. (2013) propose that polyhedral aggregates are produced during an early period of dendritic growth, followed by textural ripening. This hypothesis is based on observations that attached olivine crystals have identical orientations, are in continuous contact, and are superimposed into chains of decreasing crystal size elongated along <100> (Welsch et al., 2013). However, crystallographic branching in dendrites (Cody and Cody, 1995; Faure et al., 2003a, 2003b) is associated with misorientations lower than ~3˚ (Faure et al., 2003b), so cannot account for the 86% of olivine aggregates with misorientations >3˚ (Fig. 3). Additionally, neighbouring crystals in the subset of olivine aggregates displaying small misorientations (<5˚) were often separated by pockets of melt, and showed no preferential elongation direction or size ordering (Fig. 1a). While the textural maturation of non-crystallographic branching dendrites (Donaldson, 1976; Keith and Padden, 1963) could produce the 86% of aggregates with large misorientation angles, the crystallographic signatures of branching olivine dendrites from West Greenland Picrites differ from those of olivine aggregates (Supplementary Fig. DR5; DR1) Larsen and Pederson, 2000). While olivine dendrites and aggregates both display a misorientation angle peak at <20˚, dendrites show no peaks at higher angles (Supplementary Fig. DR5). The differences between these distributions are statistically significant (p=0.013; Kolmogorov-Smirnov test). Additionally, misorientation axes in branching dendrites form a bimodal distribution, with a primary maximum at <010> (Donaldson, 1976) and a minor secondary maximum at <100> (Supplementary Fig. DR5). This contrasts with the strong clustering of olivine misorientation axes at <100> in Kīlauean aggregates (Fig. 3b). Overall, the crystallographic and textural signatures of olivine aggregation are inconsistent with an origin from non-crystallographic branching during dendritic growth.

CONCLUSIONS

The large range of misorientations in chromite and olivine aggregates cannot be explained by crystal growth processes, which favour specific crystallographic relationships. Observed facial attachments and compositional profiles across adjacent olivines are consistent with crystal aggregation by synneusis shortly before eruption. In crystal populations affected by synneusis, textural investigations such as crystal size distributions must be constructed from measurements of individual grains within an aggregate. Consideration of the total size of an aggregate is only justified if aggregation can be attributed to twinning or dendritic growth. To

distinguish between these cases routinely, a workflow could be developed whereby the origin of grain aggregation is assessed by EBSD maps, which are subsequently used to generate “informed” CSDs. The random crystallographic relationships between adjacent chromite grains in our sample of the UG2 chromitite layer are best explained by the formation of touching networks following crystal settling. Settling as individual crystals rather than aggregates has implications for initial mush porosity and accumulation timescales, with relevance to the formation of economically-viable platinum group element deposits.

ACKNOWLEDGEMENTS

We thank Giulio Lampronti and Iris Buisman for help collecting and interpreting electron backscatter diffraction and electron microprobe microanalyzer data, and Eric Dowty for providing guidance on the use of SHAPE software. Isobel Sides (funded by a NERC studentship) and Don Swanson (United States Geological Survey) collected the Kīlauea scoria samples. Lotte Larsen and Ilya Veksler are thanked for providing the Greenland picrites and UG2 chromitite samples respectively. Wieser is funded by NERC doctoral training parternship (DTP) studentship NE/L002507/1, Vukmanovic by Marie Curie Grant 708131-EFOX-H2020-MSCA-IF-2015.

REFERENCES

Azevedo, S. and Nespolo, M., 2017. Twinning in olivine group revisited. European Journal of Mineralogy, *29*(2), pp.213-226.

Bachmann, F., Hielscher, R. and Schaeben, H., 2010. Texture analysis with MTEX–free and open source software toolbox. In Solid State Phenomena (Vol. 160, pp. 63-68). Trans Tech Publications. https://doi.org/10.4028/www.scientific.net/SSP.160.63

Brandon, D.G., 1966. The structure of high-angle grain boundaries. Acta metallurgica, 14(11), pp.1479-1484. https://doi.org/10.1016/0001-6160(66)90168-4

Brugger, C.R. and Hammer, J.E., 2015. Prevalence of growth twins among anhedral plagioclase microlites. American Mineralogist, 100(2-3), pp.385-395.

Bruno, M., Massaro, F.R., Prencipe, M., Demichelis, R., De La Pierre, M. and Nestola, F., 2014. Ab Initio calculations of the main crystal surfaces of forsterite (Mg2SiO4): a preliminary study to understand the nature of geochemical processes at the olivine interface. The Journal of Physical Chemistry C, 118(5), pp.2498-2506.

Buerger, M.J., 1945. The genesis of twin crystals. American Mineralogist: Journal of Earth and Planetary Materials, 30(7-8), pp.469-482.

239 Campbell, I.., 1978. Some problems with the cumulus theory. Lithos 11(4), pp. 311–323.
240 https://doi.org/10.1016/0024-4937(78)90038-5

241 Cody, A.M. and Cody, R.D., 1995. Dendrite formation by apparent repeated twinning of
242 calcium oxalate dihydrate. Journal of crystal growth, 151(3-4), pp.369-374.
243 https://doi.org/10.1016/0022-0248(94)00964-3

244 Day, J.M. and Taylor, L.A., 2007. On the structure of mare basalt lava flows from textural
245 analysis of the LaPaz Icefield and Northwest Africa 032 lunar meteorites. Meteoritics &
246 Planetary Science, 42(1), pp.3-17. https://doi.org/10.1111/j.1945-5100.2007.tb00213.x

247 Deer, W.A., 1966. An introduction to the rock-forming minerals. London, Longman.

248 Dodd, R.T. and Calef, C., 1971. Twinning and intergrowth of olivine crystals in chondritic
249 meteorites. Mineralogical Magazine, 38(295), pp.324-327.
250 https://doi.org/10.1180/minmag.1971.038.295.06

251 Donaldson, C.H., 1976. An experimental investigation of olivine morphology. Contributions to
252 Mineralogy and Petrology, 57(2), pp.187-213. https://doi.org/10.1007/BF00405225

253 Dowty, E., 1980a. Synneusis reconsidered. Contributions to Mineralogy and
254 Petrology, 74(1), pp.75-84. https://doi.org/10.1007/BF00375491

255 Dowty E., 1980b. Computing and drawing crystal shapes. American Mineralogist, 65,
256 pp.465-471.

257 Enderlein, J., 1997. A package for displaying crystal morphology. Mathematica Journal, 7(1),
258 pp.72-78.

259 Faure, F., Trolliard, G., Nicollet, C. and Montel, J.M., 2003a. A developmental model of
260 olivine morphology as a function of the cooling rate and the degree of
261 undercooling. Contributions to Mineralogy and Petrology, 145(2), pp.251-263.
262 https://doi.org/10.1007/s00410-003-0449-y

263 Faure, F., Trolliard, G. and Soulestin, B., 2003b. TEM investigation of forsterite
264 dendrites. American Mineralogist, 88(8-9), pp.1241-1250.
265 https://pubs.geoscienceworld.org/ammin/article-lookup?doi=10.2138/am-2003-8-907

266 Hammer, J.E., Sharp, T.G., Wessel, P., 2010. Heterogeneous nucleation and epitaxial
267 crystal growth of magmatic minerals. Geology 38, pp. 367–370.
268 https://doi.org/10.1130/G30601.1

Holness, M.B., Vukmanovic, Z., Mariani, E., 2017a. Assessing the Role of Compaction in the Formation of Adcumulates: a Microstructural Perspective. Journal of Petrology. 58, pp.643–673. https://doi.org/10.1093/petrology/egx037

Holness, M.B., Farr, R., Neufeld, J.A., 2017b. Crystal settling and convection in the Shaint Isles Main Sill. Contributions to Mineralogy and Petrology, 171:7, https://doi.org/10.1007/s00410-016-1325-x

Jackson, E.D., 1961. Primary Textures and mineral associations in the Ultramafic zone of the Stillwater complex Montana: the petrographic features and origin of the layered chromitites, bronzitites, and harzburgites in the lower part of the Stillwater complex. US Government Printing Office.

Jerram, D.A., Cheadle, M.J. and Philpotts, A.R., 2003. Quantifying the Building Blocks of Igneous Rocks: Are Clustered Crystal Frameworks the Foundation? Journal of Petrology. 44, pp. 2033–2051. https://doi.org/10.1093/petrology/egg069

Keith, H.D. and Padden Jr, F.J., 1963. A phenomenological theory of spherulitic crystallization. Journal of Applied Physics, 34(8), pp.2409-2421. https://doi.org/10.1063/1.1702757

Kirkpatrick, R.J., 1977. Nucleation and growth of plagioclase, Makaopuhi and Alae lava lakes, Kilauea Volcano, Hawaii. Geological Society of America Bulletin, 88(1), pp.78-84. https://doi.org/10.1130/0016-7606(1977)88<78:NAGOPM>2.0.CO;2

Larsen, L.M., Pedersen, A.K., 2000. Processes in High-Mg, High-T Magmas: Evidence from Olivine, Chromite and Glass in Palaeogene Picrites from West Greenland. Journal of Petrology, 41, pp.1071–1098. https://doi.org/10.1093/petrology/41.7.1071

Leal, L.G., 1980. Particle motions in a viscous fluid. Annual Review of Fluid Mechanics, 12(1), pp.435-476. https://doi.org/10.1146/annurev.fl.12.010180.002251

Lofgren, G.E., 1983. Effect of Heterogeneous Nucleation on Basaltic Textures: A Dynamic Crystallization Study. Journal of Petrology, 24, pp.229–255. https://doi.org/10.1093/petrology/24.3.2290

Marsh, B.D., 1998. On the interpretation of crystal size distributions in magmatic systems. Journal of Petrology, *39*(4), pp.553-599. https://doi.org/10.1093/petroj/39.4.5530

McIntire, M.Z., Bergantz, G.W. and Schleicher, J.M., 2019. On the hydrodynamics of crystal clustering. Philosophical Transactions of the Royal Society A, *377*(2139). https://doi.org/10.1098/rsta.2018.0015

Mithen, J.P. and Sear, R.P., 2014. Epitaxial nucleation of a crystal on a crystalline surface. EPL (Europhysics Letters), 105(1), p.18004. https://doi.org/10.1209/0295-5075/105/18004

Naldrett, A.J., 2013. Magmatic sulfide deposits: Geology, geochemistry and exploration. Springer Science & Business Media.

Nespolo, M. and Ferraris, G., 2004. The oriented attachment mechanism in the formation of twins-a survey. European Journal of Mineralogy, 16(3), pp.401-406. https://doi.org/10.1127/0935-1221/2004/0016-0401

Philpotts, A.R., Shi, J. and Brustman, C., 1998. Role of plagioclase crystal chains in the differentiation of partly crystallized basaltic magma. Nature, 395(6700), p.343.

Prior, D.J., et al., 1999. The application of electron backscatter diffraction and orientation contrast imaging in the SEM to textural problems in rocks. American Mineralogist, *84*(11-12), pp.1741-1759.

Ross, J.V., 1957. Combination twinning in plagioclase felspars. American Journal of Science, 255(9), pp.650-655.

Schwindinger, K.R., 1999. Particle dynamics and aggregation of crystals in a magma chamber with application to Kilauea Iki olivines. Journal of Volcanology and Geothermal Research, 88(4), pp.209-238. https://doi.org/10.1016/S0377-0273(99)00009-8

Schwindinger, K.R. and Anderson, A.T., 1989. Synneusis of Kilauea Iki olivines. Contributions to Mineralogy and Petrology, 103(2), pp.187-198. https://doi.org/10.1007/BF00378504

Špillar, V. and Dolejš, D., 2015. Heterogeneous nucleation as the predominant mode of crystallization in natural magmas: numerical model and implications for crystal–melt interaction. Contributions to Mineralogy and Petrology, 169(1), p.4. https://doi.org/10.1007/s00410-014-1103-6

Turnbull, D. and Vonnegut, B., 1952. Nucleation catalysis. Industrial & Engineering Chemistry, 44(6), pp.1292-1298. https://doi.org/10.1021/ie50510a031

Vance, J.A., 1969. On synneusis. Contributions to Mineralogy and Petrology, 24(1), pp.7-29.

Vogt, J.H.L., 1921. The physical chemistry of the crystallization and magmatic differentiation of igneous rocks. The Journal of Geology, 29(4), pp.318-350. https://doi.org/10.1086/622785

Welsch, B., Faure, F., Famin, V., Baronnet, A., Bachèlery, P., 2013. Dendritic Crystallization: A Single Process for all the Textures of Olivine in Basalts? Journal of Petrology, 54, pp.539–574. https://doi.org/10.1093/petrology/egs077

Welsch, B., Hammer, J., Hellebrand, E., 2014. Phosphorus zoning reveals dendritic architecture of olivine. Geology 42, 867–870. https://doi.org/10.1130/G35691.1

FIGURE CAPTIONS

Fig. 1 – a-b) Backscatter Electron (BSE) images of olivine aggregates consisting of 3-5 crystals. Prominent areas of melt are trapped between neighbouring crystals. c-d) EBSD-derived inverse pole figure maps (IPF) of the aggregates, color-coding the crystal direction parallel to Z / image normal. For example, the crystals in c) are colored red to demonstrate that their <100> axes are close to vertical. Olivine shapes in c) were computed using the crystalShape MTEX class, allowing assessment of facial attachments. In this case, crystals are predominantly attached along {110}-{110} faces. Note the presence of a misaligned crystal in c) within an aggregate mostly formed of crystals with similar orientations. If this aggregate formed by dendritic growth, synneusis would also have to be operating. The more parsimonious explanation is that attached crystals with both high and low misorientations formed by synneusis. e) BSE images of two olivine aggregates, showing the locations of electron probe microanalyzer transects. Attached grains show different forsterite contents [Fo=100xMg/(Mg+Fe), atomic]. The presence of flat plateaus within profiles X-X' and Z-Z' demonstrates that these transects cut across grain cores, which must have grown in different conditions. These profiles are not consistent with a scenario whereby compositionally homogeneous aggregates (formed by growth processes) are altered by diffusion or late-stage growth. The presence of steep gradients in forsterite content between crystals indicates that limited diffusive re-equilibration has occurred following aggregation.

Fig. 2 -a) Transmitted light image of a small region of the UG2 chromitite (Bushveld Complex, South Africa) thin section. The chromites (black) form a prominent touching network. b) EBSD-derived inverse pole figure (IPF) map of a larger area of the thin section, color-coded as in Figure 1 (e.g. grains with their <111> axes vertical appear blue). The wide range of colors points to an absence of crystallographic preferred orientation. c) Transmitted light image of a chromite-poor pyroxenite, lying 0.5 m above the UG2 chromitite layer. Touching frameworks of chromite crystals are relatively scarce compared to the chromitite layer itself (a-b), and separated and attached chromite crystals rest on the underlying pyroxene grains. This indicates that chromites settle as isolated grains (accounting for their random orientations), with aggregates only forming when sufficient grains settle in one place.

Fig. 3– a) Schematic diagram showing the misorientation angle (80.9˚) and axis (<100>) for a hypothetical olivine aggregate. b-c) Misorientation axes and angles for 203 touching olivine crystals within 93 aggregates. Misorientation axes cluster strongly at <100>. Misorientation angles exhibit prominent peaks around the angles predicted for perfect attachment along different crystal faces (crystal aggregates drawn in SHAPE7.4; Dowty, 1980b). Small peaks close to the (011) and (012) twin laws are also present. The color scale shown in B has units of 'multiples of uniform distribution'

Fig. 4- a) Chromite misorientation axes show moderate clustering about <111> (for ~3500 chromite grains within one thin section). b) Removal of {111} twins and normalization to the theoretical axis distribution (see DR1) leaves a near-uniform axis distribution. The color scales shown in A and B has units of 'multiples of uniform distribution' c) Chromite aggregates show a wide range of misorientation angles. Removal of the prominent peak at 60˚ caused by {111} twins results in a distribution similar to the symmetry-induced distribution.

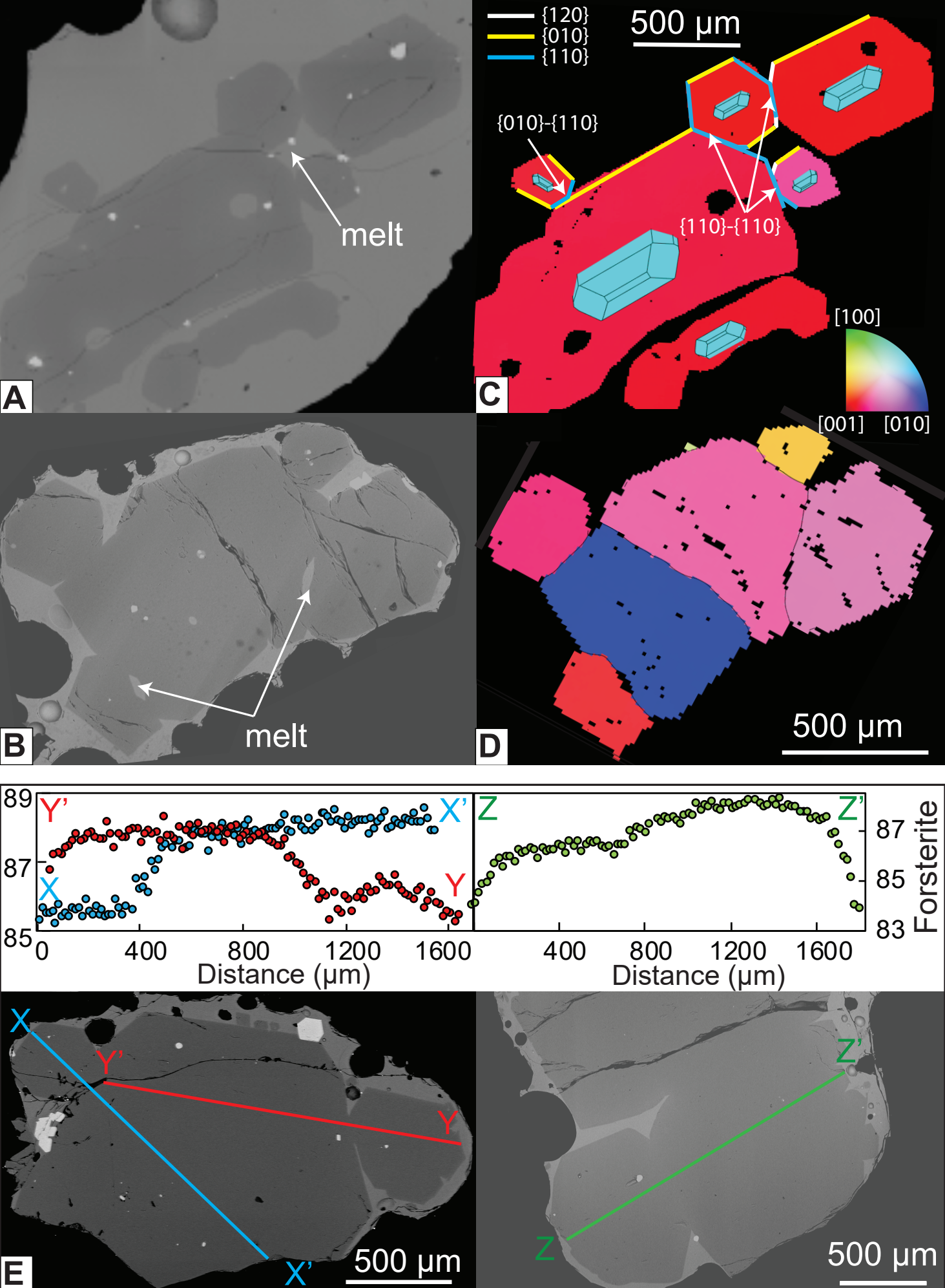
melt
A
{120}
{010}
{110}
500 µm
{010}-{110}
{110}-{110}
[100]
[001]
[010]
C
melt
B
D
500 µm
89
87
85
Y'
X'
X
Y
Z
Z'
0
400
800
1200
1600
Distance (µm)
87
85
83
Forsterite
X
Y'
Y
X'
500 µm
E
Z'
Z
500 µm

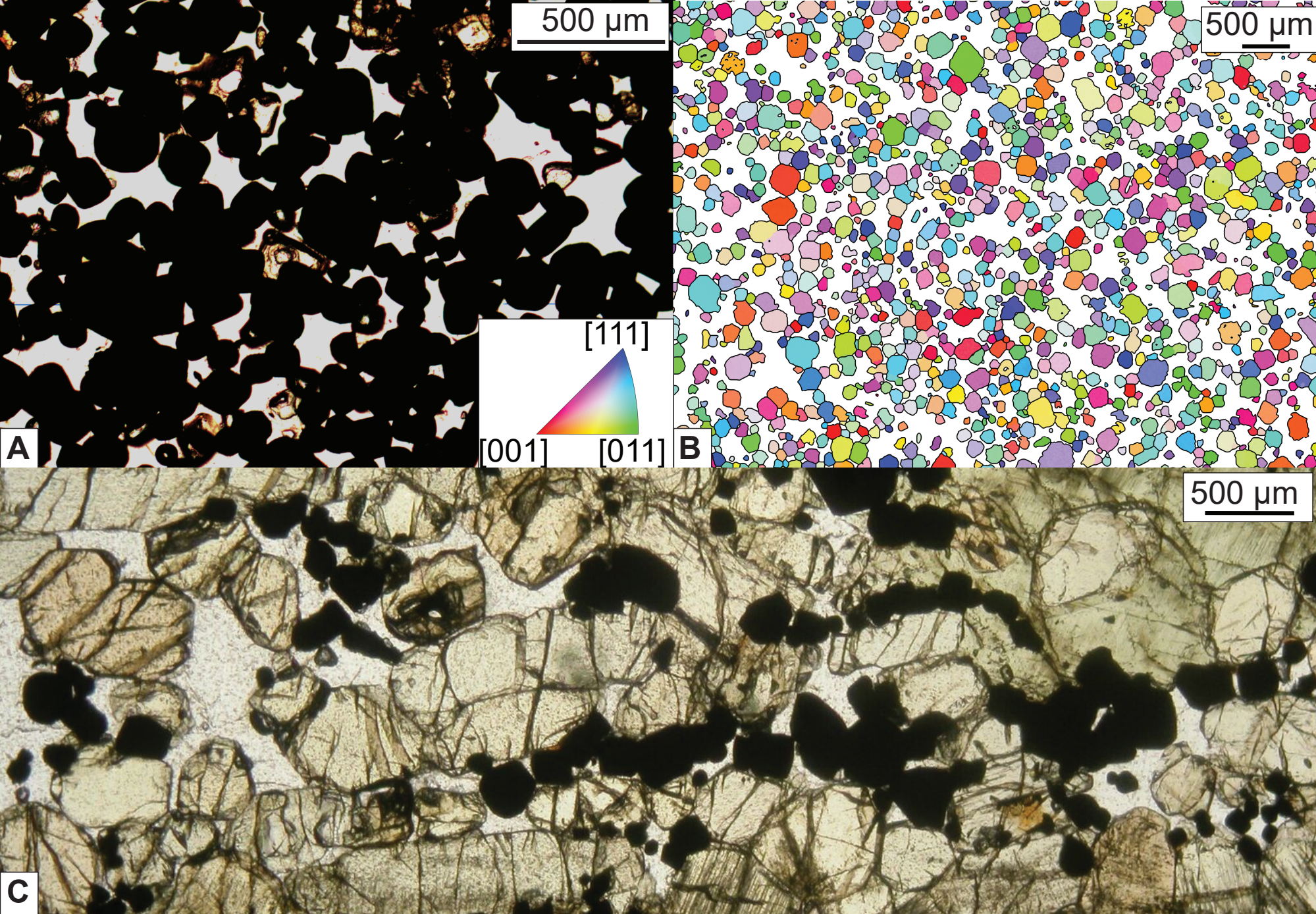
500 µm
[111]
[001]
[011]
A
500 µm
B
500 µm
C

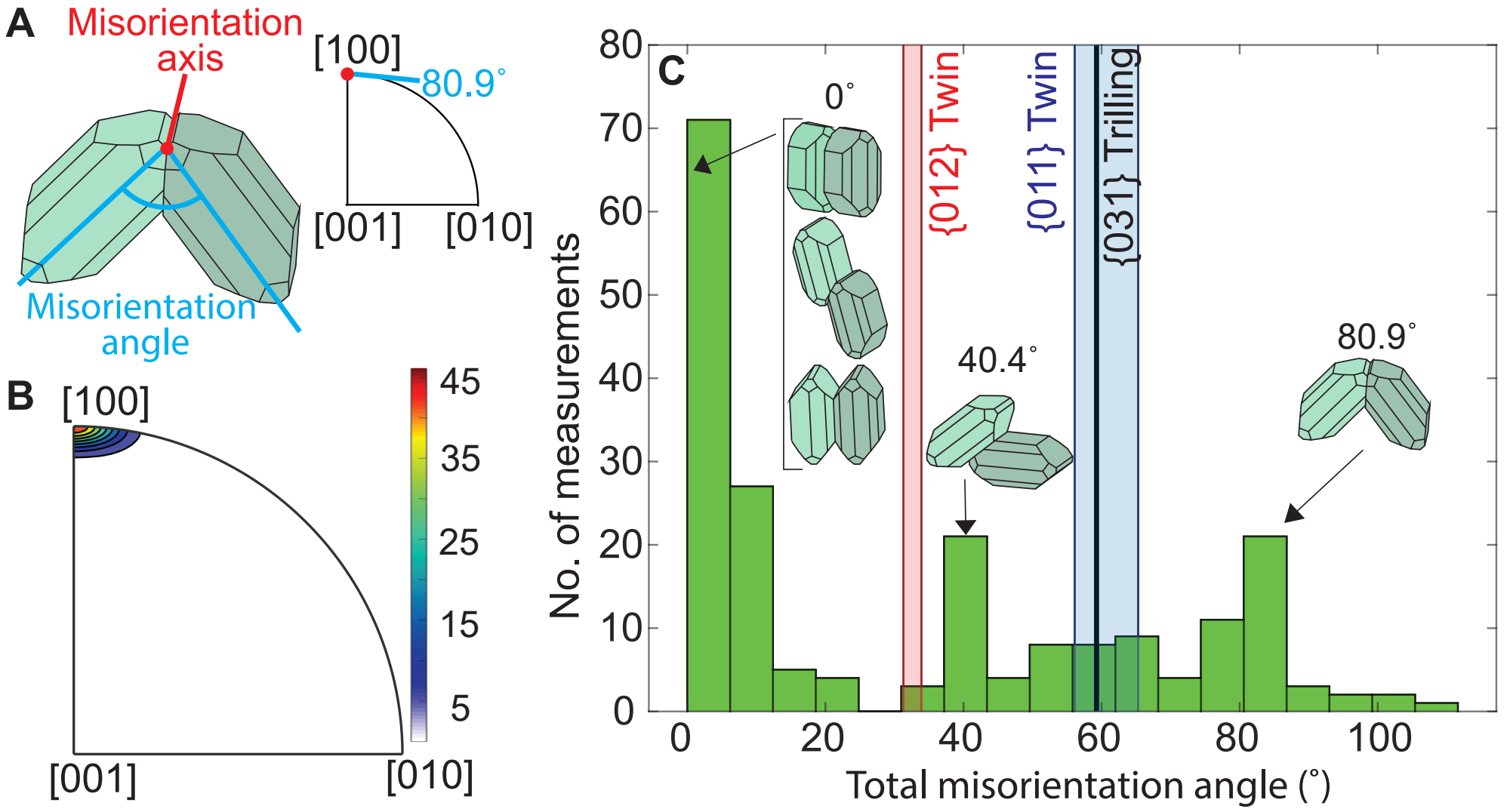
A
Misorientation axis
[100]
80.9°
[001]
[010]
Misorientation angle
B
[100]
45
35
25
15
5
[001]
[010]
C
0°
40.4°
80.9°
{012} Twin
{011} Twin
{031} Trilling
No. of measurements
Total misorientation angle (°)
0
10
20
30
40
50
60
70
80
0
20
40
60
80
100

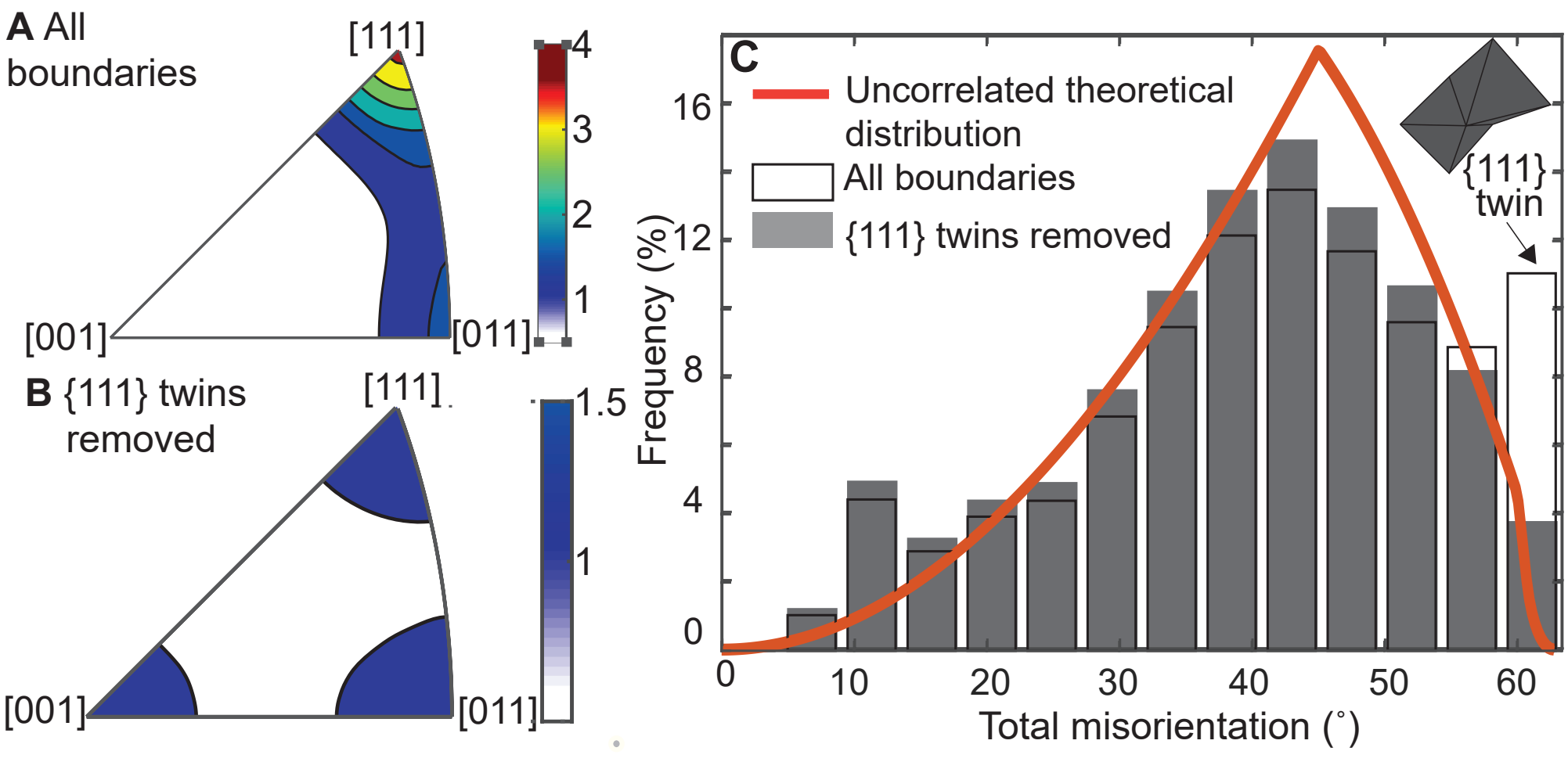
A All boundaries
[111]
[001]
[011]
4
3
2
1
B {111} twins removed
[111]
[001]
[011]
1.5
1
C
Uncorrelated theoretical distribution
All boundaries
{111} twins removed
{111} twin
Frequency (%)
16
12
8
4
0
0
10
20
30
40
50
60
Total misorientation (˚)

DATA REPOSITORY 1

To Sink, Swim, Twin or Nucleate: A critical appraisal of crystal aggregation processes

Penny E. Wieser[1*], Zoja Vukmanovic[1], Rüdiger Kilian[2], Emilie Ringe[1,3], Marian B. Holness[1], John Maclennan[1], Marie Edmonds[1]

[1] Department of Earth Sciences, University of Cambridge, CB2 3EQ, UK.

[2] Department of Environmental Sciences, University Basel, Switzerland.

[3]Department of Materials Science and Metallurgy, University of Cambridge, CB3 OFS, UK.

* Corresponding author: pew26@cam.ac.uk

SAMPLE LOCATIONS

The UG2 chromitite sample was kindly provided by Ilya Veksler. This was collected from the Rustenburg layered suite at Khuseleka mine (25°37'26.73"S, 27°15'22.11"E; see Veksler et al. 2018 for more details).

Olivine dendrites within West Greenland picritic samples were kindly provided by Lotte Larsen (see Larsen and Pederson, 2000 for more details).

Olivine aggregates were analysed from a variety of subaerial eruptions at Kīlauea volcano (see below). The samples are from Kilauea's East Rift Zone (ERZ), the northern and southern strand of the South West Rift Zone (NSWRZ; SSWRZ), and around the summit caldera (intracaldera if within the summit depression, extracaldera if around the bordering faults).

Sample	Number of aggregates examined	Eruption Date	Location	GPS co-ordinates
KL0909	4	May 24th, 1969	ERZ	19˚ 21.826‘ N, 155˚ 12.877‘ W
KL0908	29	Dec 30th, 1969	ERZ	19˚ 20.839‘ N, 155˚ 12.518‘ W
KL0910	13	Nov 10th, 1973	ERZ	19˚ 22.313‘ N, 155˚ 13.510‘ W
KL0916	1	Aug 14th, 1971	Intracaldera	19˚ 24.137‘ N, 155˚ 16.644‘ W
KL0917	2	Late July, 1974	Intracaldera	19˚ 21.06‘ N, 155˚ 16.653‘ W
KL0919	5	Late Dec, 1974	SSWRZ	19˚ 22.649‘ N, 155˚ 17.609‘ W
KL0920	5	Late Dec, 1974	SSWRZ	19˚ 22.603‘ N, 155˚ 17.713‘ W
KL0921	7	~1700 AD	SSWRZ	19˚ 22.989‘ N, 155˚ 17.464 ‘W
KL0924	10	Late July, 1974	Extracaldera	19˚ 24.142’ N, 155˚ 16.896’ W
KL0930	15	1919-1920	NSWRZ	19˚ 21.230’ N, 155˚ 23.892’ W
KL0931	2	Sept 24-29th, 1971	NSWRZ	19˚ 20.625’ N, 155˚ 21.659’ W

SAMPLE PREPARATION

The vesicular nature of the basaltic scoria samples from Kīlauea Volcano was not amenable to thin section making. Additionally, due to the high modal proportion of vesicles, few olivines were found within each thin section. Instead, olivines were picked from sieved, jaw crushed material, and mounted in epoxy stubs. Aggregates were identified from the external morphology of crystals in backscatter electron maps. Samples from the UG2 chromitite layer and West Greenland Picrites were made into thin sections.

Epoxy stubs and thin sections were polished with progressively finer silicon pastes, then with colloidal silica using a VibroMet 2 Buehler Vibratory Polisher. A thin carbon coat was applied before EBSD analysis, and a thicker carbon coat was applied for olivine EPMA analysis.

EBSD-CHROMITE AGGREGATES

EBSD data was collected on a FEI sFEG XL30 SEM with an Oxford Nordlys HKL detector in the Department of Physics, University of Cambridge.

SEM Settings		**EBSD Settings**	
Aperature	*3*		
Voltage	*20kV*	Background (frames)	*64*
Beam Size	*5*	Gain	*10*
Sample Tilt	*70˚*	Hough Resolution	*60*
Working Distance	*20mm*	Band Detection (min/max)	*6/7*
Step size	*15µm*	Reference	*Chromite.cry (Aztec database)*

ESBD-OLIVINE AGGREGATES

EBSD data was collected on a FEI Quanta 650FEG SEM equipped with a Bruker e-Flash HR EBSD detector in the Department of Earth Sciences, University of Cambridge. Data collection and indexing was performed with Bruker QUANTAX CrystaAlign. Step size was varied depending on the size of the aggregate so that each map took ~15-20 mins to collect.

SEM Settings		**EBSD Settings**	
Aperture	*3*	Sample-Detector Distance	*~14mm*
Voltage	*20kV*	Background (frames)	*2*
Beam Size	*5.5*	Gain	*10-30*
Sample Tilt	*70˚*	Hough Resolution	*60*
Working Distance	*~17-14mm*	Band Detection (min/max)	*6/12*
Step size	*3-15µm*	Reference	Forsterite (Fe 0.2 MgO 1.8) AMSDB-ID: 0008912
		EBSP resolution	*320x240 pixels*

EPMA-OLIVINE AGGREGATES

Olivine transects were performed using a Cameca SX100 EPMA in the Department of Earth Sciences, University of Cambridge. Run conditions of 15kv and 20nA were used, with a beam size of 1µm. Count times, calibration materials, and estimates of precision and accuracy calculated from repeated measurements of a San Carlos Olivine secondary standard are shown below.

Element	Calibration Material	Crystal	Peak Count Time	Precision (%) (Std dev/mean)	Accuracy (%) (measured/standard)
Al	Corundum	LTAP	60s	12.3	97.65
Ca	Diopside	PET, LPET	60s, 60s	6.43	93.55
Si	Diopside	TAP	10s	0.85	99.62
Mg	St. Johns Olivine	TAP	20s	0.75	99.06
Fe	Fayalite	LIF	20s	1.83	99.61

EBSD DATA PROCESSING

Calculating Misorientations

Slightly different methods were used to calculate the misorientation between adjacent grains within olivine and chromite aggregates, reflecting the fact that thousands of chromites were present within a single thin section, whereas olivines aggregates were mounted separately in epoxy, and mapped individually.

For a single EBSD map of an olivine aggregate, grains were calculated using the MTEX calcGrains function with a threshold angle of 0.5˚. The positions of the resulting grain boundaries were then compared to BSE images, and only those separating morphologically distinct grains were selected, discarding low angle boundaries in the interior of grains. Then, misorientations were calculated by comparing the mean orientation of adjacent grains selected by the user (Fig. DR1). The traditional approach of calculating misorientations along grain boundaries was not used due to the common presence of residual melt along boundaries. For each map, the resulting misorientation axis and angle were saved as a MATLAB variable. These variables were then combined for 203 touching grains within 93 aggregates to plot the resulting contoured axis and angle distributions shown in Fig. 3. The same methodology was used to assess the misorientation signature of olivine dendrites (Fig. DR5).

In contrast, chromite neighbour pair misorientation measurements were calculated automatically from a single EBSD map of the entire thin section. Due to the presence of thousands of individual chromites in a single EBSD map, a higher threshold for the grain segmentation was used (8˚), to automatically separate high and low angle grain boundaries.

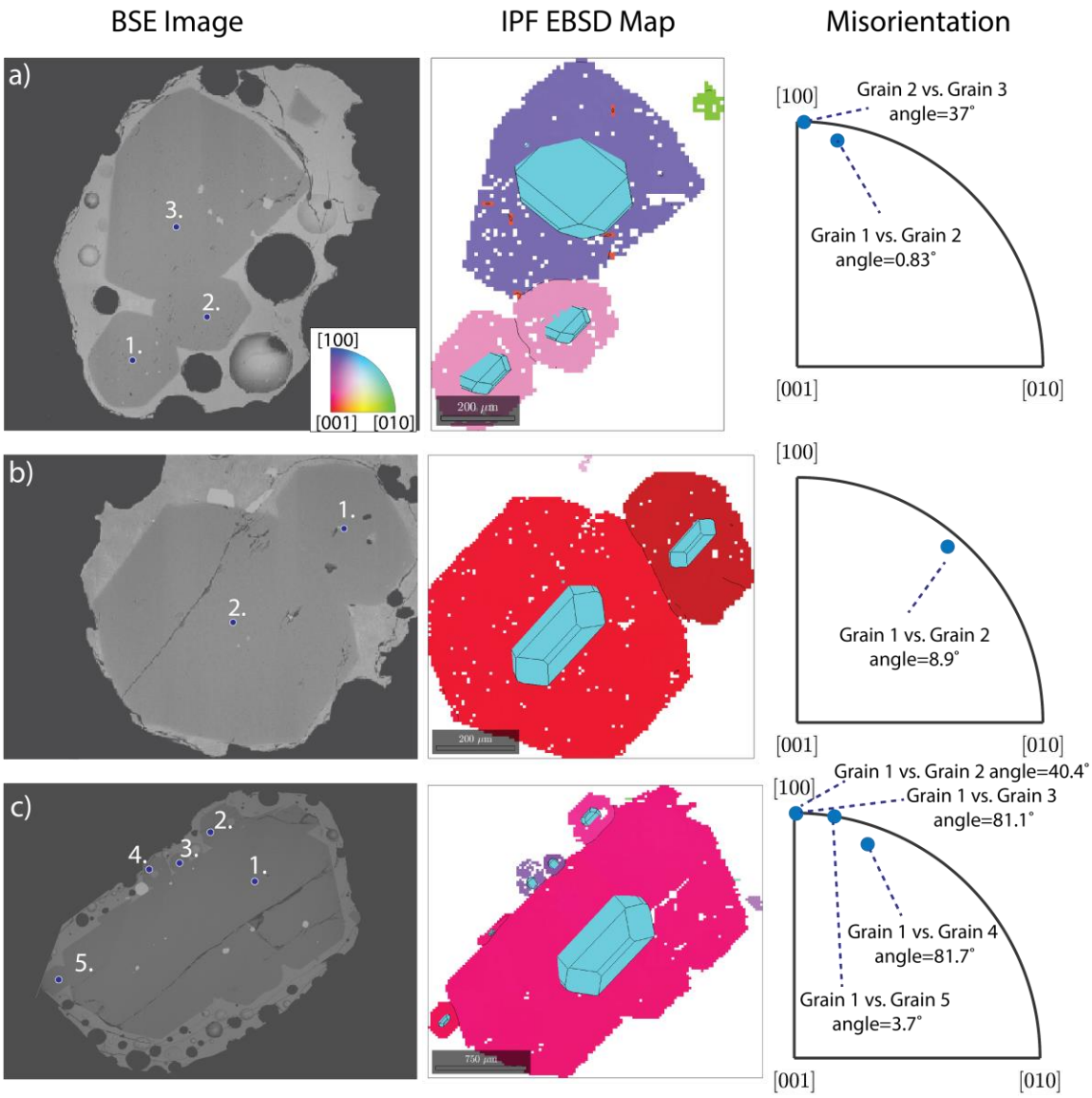

Fig. DR1 –Examples of the method used to quantify misorientations within individual olivine aggregates. BSE images (LHS) were used to identify boundaries between morphologically distinct crystals. EBSD maps (middle) are colored with respect to their orientation (e.g. red colors shows that the [001] axis is normal to the image plane). The orientation of each crystal can also be visualized from the 3D olivine shape superimposed in MTEX. Misorientations for each pair of touching grains are shown as axis-angle pairs (RHS). Individual measurements from 93 separate EBSD maps were combined to produce Fig. 3 in the main text.

Normalising Misorientation Axes in Chromite aggregates

The density distribution of misorientation axes over the full angle range is not uniform for all crystallographic directions, even for uniformly distributed crystal orientations. This is due to the non-uniform misorientation angle distribution (i.e. the maximum misorientation angle). For example, for chromites, the maximum angle about <100> is 45°, about <111> is 60°, while the maximum possible misorientation angle of 62.8° in a cubic system can only be realised around ~<773>. Accordingly, misorientation axis close to <773> have a higher probability of being encountered than other axes in a random sample of misorientations

drawn from a uniform distribution. In contrast, axes with a smaller angular range (e.g. <100>) will have a lower probability density. The non-uniform misorientation axis distribution is defined purely by the crystal symmetry, rather than the characteristics of the sample. Thus, the measured misorientation axis distribution should be normalized to this. Normalisation was performed by computing the spherical functions for each misorientation axis distribution, and dividing the measured distribution by this uniform-derived function, and normalising to a mean density of 1. This correction is particularly important in high symmetry minerals, such as chromite. For simplicity, olivine axes were left unnormalized, as the clustering of misorientation axes was so strong that normalizing to the uniform axis distribution was not significant.

Identifying Twin Laws

To identify potential twins in aggregates, a criterion was required to specific the permitted deviation from the ideal twin laws (Fig. DR2).

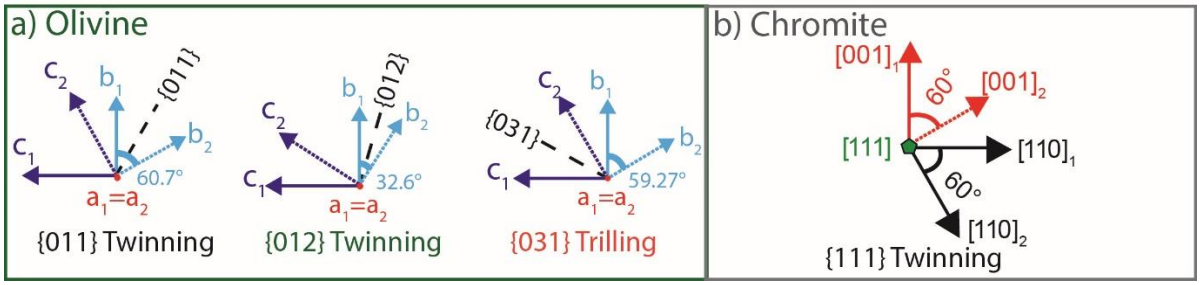

Fig. DR2 -Twin laws in olivine and chromite, after Dodd and Calef, 1971) and Deer (1966) respectively.

Crystals of cubic minerals such as chromites exhibit a special type of low energy boundary called coincidence site lattices (CSLs), where a finite number (Σ) of lattice points coincide along the boundary (Randle and Engler, 2000). The chromite twin law is the most common CSL with Σ = 3 (Garbacz and Grabski, 1989). The permitted deviation from these ideal CSLs (or twins) was calculated using Brandons Law:

$$\vartheta = \vartheta_0 (\Sigma)^{-0.5}$$

where ϑ is the permitted deviation, ϑ_0 is the angle used to differentiate subgrain and true grain boundaries (8˚), and Σ is the CSL number.

For the {111} twin in chromites (CSL3), the permitted deviation is 4.61˚. The application of Brandon's law (and thus CSL numbers) to systems with lower symmetry such as olivine is less well established. As an approximation, CSL numbers can be calculated based on the hexagonal cubic sublattice for planes of oxygen within olivine (Poirier, 1975). Using Σ=3 for {011} twinning, and Σ=39 for {012} twinning (Faul and Fitz Gerald, 1999), this permits angular deviations of 4.6˚ and 1.3˚ respectively from the idea twin laws (when ϑ_0=8˚).

Assessing Facial Attachments using crystalShape

The crystalShape MTEX class was used to superimpose 3D olivine crystals on 2D EBSD maps (https://mtextoolbox.github.io/files/doc/crystalShape_index.html).This, alongside BSE images showing the euhedral outlines of grains, allows assessment of facial attachments in approximately ~50% of aggregates (those with euhedral-subhedral crystal shapes). For examples, see Fig 1 in the text, and Fig. DR1 above.

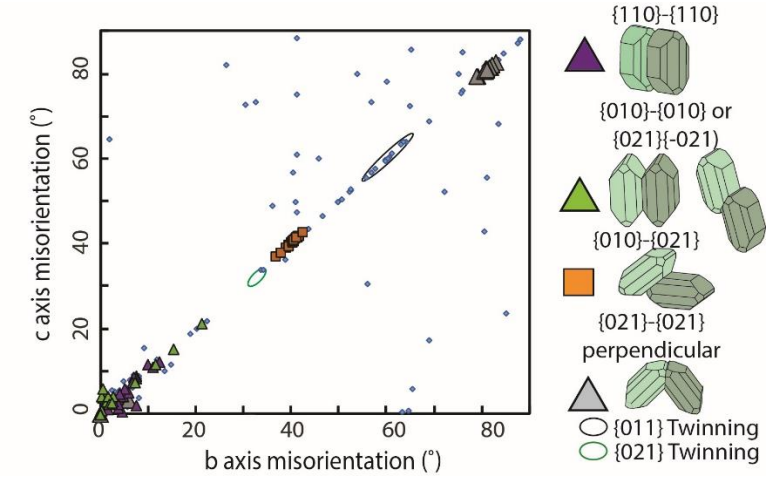

Fig. DR3 – There is an excellent correlation between the misorientation of the b and c axes of neighbouring crystals in olivine aggregates (resulting from the clustering of misorientation axes about <100>). Grains where facial attachments could be assessed are indicated. Grains within the permitted deviation of olivine twin laws are circled.

CALCULATING SURFACE ENERGIES

SHAPE V7.4 (www.shapesoftware.com) was used to construct euhedral olivine and chromite crystals of known facial areas and volumes. For olivine, forsterite unit cell parameters were used (a=4.756, b=10.195, c=5.981 Å). The shape ratio was set at a:b:c=1.5:1:2, with the central distances ratios used by Welsch et al. (2013). For cubic chromite, only {111} faces were expressed. Central distances were adjusted to produce a crystal with a volume of 1mm^3 (Fig. DR4).

The interfacial energy for a single crystal with a volume of 1mm^3 was calculated by multiplying the area of each face by the interfacial energy of that face. Central distances were then adjusted to yield a crystal with a volume of 0.5mm^3 . The total interfacial energy of two attached 0.5mm^3 crystals was calculated by multiplying the area of each face by its energy, minus the energies of the two attached faces.

For chromite, surface energies for $NiFe_2O_4$ spinel from Mishra and Thomas (1977) were used. However, as only {111} faces are expressed, the ratio of aggregate:single crystal energies for chromite is not dependent on the choice of surface energy. For olivine, Ab initio surface energies of forsterite in a vacuum at 0 K were used (Bruno et al., 2014). As surface adsorption on olivine in basaltic melt is anisotropic (Wanamaker and Kohlstedt, 1991; de Leeuw et al., 2000), our calculated energy differences are reliant on the assumption that the relative magnitudes of facial energies are not affected by surface adsorption. However, as there are significant energy penalties for growth of a daughter crystal for all attachment faces, the conclusion that heterogeneous nucleation is energetically unfavourable is not sensitive to the exact choice of facial energies.

Table 1a – Calculations for single olivine crystal with a volume of 1mm^3 (morphology shown in Fig. DR4)

Face	**Energy** *(J/m^2)*	**Number of faces**	**Total face area** *Area of each face (mm^2)x # of faces*	**Total energy per face (μJ)** *Energy (J/m^2)xArea (mm^2)*
010	1.22	2	1.109	1.353
021	1.90	4	2.023	3.843
110	2.18	4	1.438	3.135
101	1.78	4	0.179	0.319
001	1.78	2	0.176	0.313
120	1.36	4	0.683	0.928
Total interfacial energy (sum of all 6 faces)				**9.89 μJ**

Table 1b– Calculation of the interfacial energy for an olivine aggregate consisting of two identical crystals (each with a volume of 0.5mm^3) joined along the {010} face.

Face	**Energy** *(J/m^2)*	**Number of faces**	**Total face area** *Area of each face (mm^2)x # of faces*	**Total energy per face (μJ)** *Energy (J/m^2)xArea (mm^2)*
010	1.22	2	0.699	0.853
021	1.90	4	1.274	2.421
110	2.18	4	0.906	1.975
101	1.78	4	0.113	0.201
001	1.78	2	0.111	0.197
120	1.36	4	0.430	0.585
Total interfacial energy per crystal				**6.23 μJ**
Interfacial energy of two 010 faces				**0.853 μJ**
Total interfacial energy of aggregate *2 x Total energy per crystal – energy of 2 touching 010 faces*				**11.6 μJ**
aggregate energy/single crystal energy (%)				**117%**

Table 1c- Energy differences for aggregates joined along each of the 6 olivine crystal faces.

Attached Faces	**{110}**	**{120}**	**{010}**	**{021}**	**{001}**	**{101}**
aggregate energy/single crystal energy (%)	116%	123%	117%	114%	124%	125%

Table 1d– Calculations for single chromite crystal with a volume of 1mm^3 (morphology shown in Fig. DR4)

Face	**Energy** *(J/m^2)*	**Number of faces**	**Total face area** *Area of each face (mm^2)x # of faces*	**Total energy per face (μJ)** *Energy (J/m^2)xArea (mm^2)*
{111}	0.207	8	5.719	1.184
Total interfacial energy				**1.18 μJ**

Table 1e– Calculation of the interfacial energy for a chromite aggregate consisting of two identical crystals (each with a volume of 0.5mm^3) joined along the {111} face.

Face	**Energy** *(J/m^2)*	**Number of faces**	**Total face area** *Area of each face (mm^2)x # of faces*	**Total energy per face (μJ)** *Energy (J/m^2)xArea (mm^2)*
{111}	0.207	8	3.603	0.746
Total interfacial energy per crystal				**0.746 μJ**
Interfacial energy of two 111 faces				**0.186 μJ**
Total interfacial energy of aggregate *2 x Total energy per crystal – energy of 2 touching 111 faces*				**1.31 μJ**

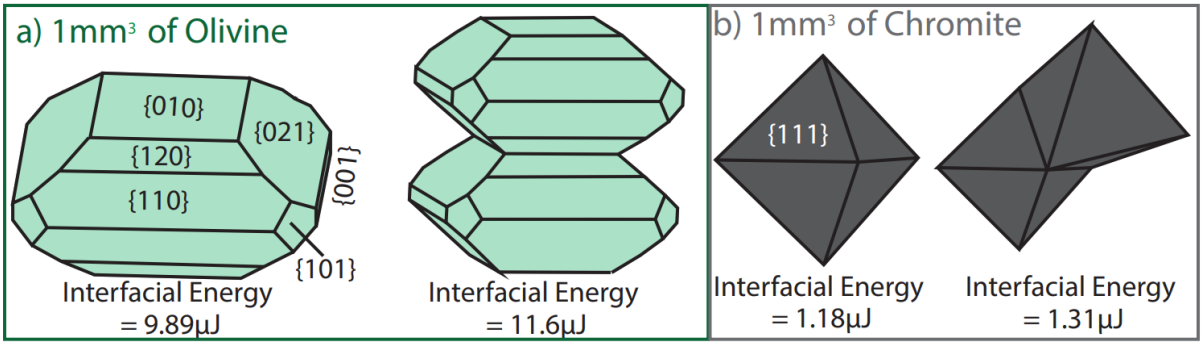

Fig DR4– Crystal geometries used for interfacial energy calculations (produced in SHAPE V7.4).

MISORIENTATION SIGNATURES OF OLIVINE DENDRITES

Misorientations in branching olivine dendrites from West Greenland Picrites (Larsen and Pederson, 2000) were quantified to assess whether olivine aggregates represent texturally matured dendrites (as suggested by Welsch et al., 2013).

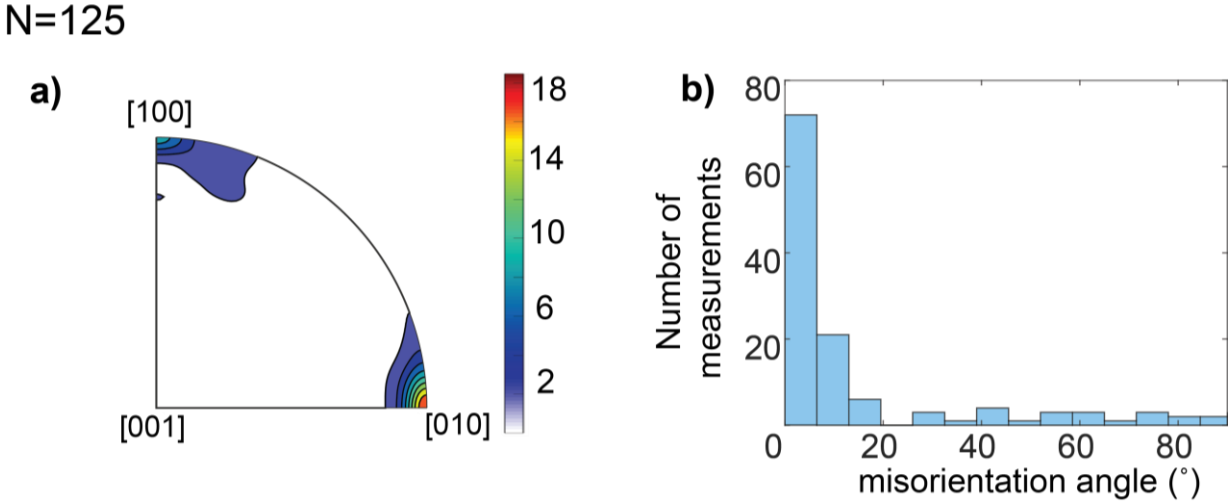

Fig DR5– a) Misorientation axes for 125 dendritic buds displaying non crystallographic branching cluster strongly at [010] (as reported by Donaldson, 1976), with a weak secondary maxima at [100] (previously unreported). The color scale in a) has units of 'multiples of uniform distribution'. b) Misorientation angles show a peak at <10˚, but a relatively uniform distribution at higher angles. This is in clear contrast to the multiple misorientation peaks observed in Kīlauean aggregates.

ADDITIONAL REFERENCES

Bruno, M., Massaro, F.R., Prencipe, M., Demichelis, R., De La Pierre, M. and Nestola, F., 2014. Ab Initio calculations of the main crystal surfaces of forsterite (Mg2SiO4): a preliminary study to understand the nature of geochemical processes at the olivine interface. The Journal of Physical Chemistry C, 118(5), pp.2498-2506.

De Leeuw, N.H., Parker, S.C., Catlow, C.R.A. and Price, G.D., 2000. Modelling the effect of water on the surface structure and stability of forsterite. Physics and Chemistry of Minerals, 27(5), pp.332-341.

Faul, U.H. and Gerald, J.D.F., 1999. Grain misorientations in partially molten olivine aggregates: an electron backscatter diffraction study. Physics and Chemistry of Minerals, 26(3), pp.187-197.

Garbacz, A., and M. W. Grabski. 1989. Modelling of CSL boundaries distribution in polycrystals. Scripta metallurgica 23(8), pp. 1369-1374.

Poirier, J.P., 1975. On the slip systems of olivine. Journal of Geophysical Research, 80(29), pp.4059-4061.

Mishra, R.K. and Thomas, G., 1977. Surface energy of spinel. Journal of Applied Physics, 48(11), pp.4576-4580.

QUANTAX CrystAlign. Bruker Nano GmbH, Berlin, Germany, 2010.

Randle, V. and Engler, O., 2000. Introduction to Texture Analysis: Macrotexture, Microtexture and Orientation Mapping. Gordon & Breach Science Publishers. Reading, UK.

Veksler, I.V., Sedunova, A.P., Darin, A.V., Anosova, M.O., Reid, D.L., Kaufmann, F.E., Hecht, L. and Trumbull, R.B., 2018. Chemical and textural re-equilibration in the UG2 chromitite layer of the Bushveld Complex, South Africa. Journal of Petrology.

Wanamaker, B.J. and Kohlstedt, D.L., 1991. The effect of melt composition on the wetting angle between silicate melts and olivine. Physics and Chemistry of Minerals, 18(1), pp.26-36. https://doi.org/10.1007/BF00199040